

# Surprising lateral interactions between negatively charged adatoms on metal surfaces

Matic Poberžnik and Anton Kokalj\*

Department of Physical and Organic Chemistry, Jožef Stefan Institute, Jamova 39, SI-1000 Ljubljana, Slovenia

May 1, 2020

## Abstract

Even something as conceptually simple as adsorption of electronegative adatoms on metal surfaces, where repulsive lateral interactions are expected for obvious reasons, can lead to unanticipated behavior. In this context, we explain the origin of surprising lateral interactions between electronegative adatoms observed on some metal surfaces by means of density functional theory calculations of four electronegative atoms (N, O, F, Cl) on 70 surfaces of 44 pristine metals. Four different scenarios for lateral interactions are identified, some of them being unexpected: (i) they are repulsive, which is the typical case and occurs on almost all transition metals. (ii,iii) They are atypical, being either attractive or negligible, which occurs on p-block metals and Mg, and (iv) surface reconstruction stabilizes the low-coverage configuration, preventing atypical lateral interactions. The last case occurs predominantly on s-block metals.

---

ORCID IDs: 0000-0002-4866-4346 (MP), 0000-0001-7237-0041 (AK)

\* Corresponding Author: Anton Kokalj, Tel: +386-1-477-35-23; Fax: +386 1 251 93 85, E-mail: tone.kokalj@ijs.si, URL: <http://www.ijs.si/ijsw/K3-en/Kokalj>

## INTRODUCTION

The adsorption of electronegative atoms on metal surfaces is of paramount importance in surface science as well as electrochemistry.<sup>1-4</sup> As an electronegative atom approaches a metal surface, charge is transferred and it becomes negatively charged. This interaction can be described classically by the method of images, where the adatom/image-charge pair can be seen as a dipole. As more adatoms accumulate on the surface repulsive interactions are expected between them. Such interactions were confirmed for a variety of adatoms on metal surfaces<sup>5-11</sup> and they typically scale as  $\mu^2/R^3 \propto \mu^2\Theta^{\frac{3}{2}}$ , where  $\mu$  is the adatom induced dipole,  $R$  is the nearest-neighbor interadatom distance, and  $\Theta$  is the surface coverage. However, in a few cases, notably for electronegative atoms on Mg(001)<sup>12,13</sup> and O on Al(111),<sup>14-16</sup> counterintuitive attractive interactions were identified. In our previous publication<sup>16</sup> we explained that these surprising attractive lateral interactions are a consequence of the interplay between electrostatic and geometric effects and that there exists a critical height of adatoms above the surface, below which attractive interactions can emerge. Since this model—

explained in the Supporting Information and henceforth referred to as the simple ionic model—requires only (i) sufficiently ionic bonding and (ii) a low height of the adatom above the surface, it stands to reason that it should be generally applicable, provided that the two requirements are met. To address this proposition, the adsorption of four different electronegative adatoms (N, O, F, and Cl) on 44 elemental metals, as indicated in Figure 1, is considered herein by means of density-functional-theory (DFT) calculations.

## TECHNICAL DETAILS

DFT calculations were performed with the `PWscf` code from the `Quantum ESPRESSO` distribution<sup>17</sup> and the `PWTK` scripting environment,<sup>18</sup> using the generalized gradient approximation (GGA) of Perdew–Burke–Ernzerhof (PBE).<sup>19</sup> We used the projector augmented wave (PAW) method<sup>20</sup> with PAW potentials obtained from a pseudopotential library.<sup>21,22</sup> Kohn–Sham orbitals were expanded in a plane wave basis set with a kinetic energy cutoff of 50 Ry (600 Ry for the charge density). Brillouin zone (BZ) integrations were performed with the special point technique,<sup>23</sup> using a  $12 \times 12 \times 1$  shifted  $k$ -mesh for  $(1 \times 1)$  surface cells (or equivalent for larger cells) and a Methfessel–Paxton smearing<sup>24</sup> of 0.02 Ry. Molecular graphics were produced by the `XCrySDen` graphical package.<sup>25</sup>

Most of the investigated metals crystallize in one of the following three lattice types: face-centered-cubic (fcc), hexagonal-close-packed (hcp), and body-centered-cubic

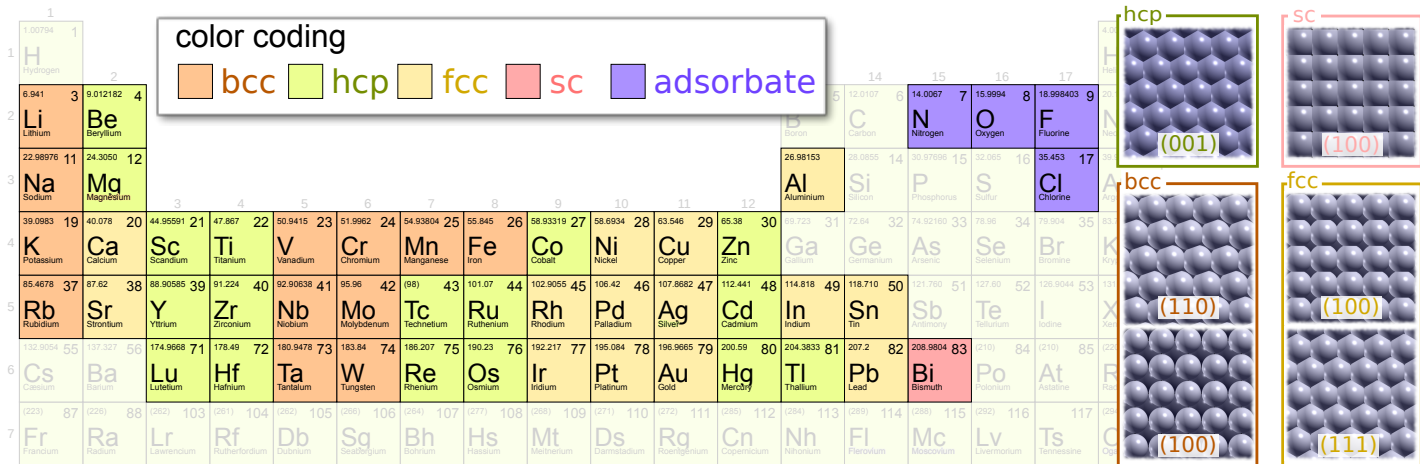


**Figure 1.** The investigated metals and adsorbates are highlighted in the periodic table. The lattice type of each investigated metal is indicated by the color coding; note that metals with exotic lattices were modeled as either bcc, fcc, hcp, or simple-cubic (sc) as explained in the text. The side panel displays topviews of the considered surfaces for each lattice type.

(bcc). The exceptions are In and Sn, which crystallize in tetragonal lattices, as well as Hg and Bi, which crystallize in rhombohedral lattices. For these metals the most stable among fcc, hcp, bcc, or simple-cubic (sc) was chosen as the representative model in order to simplify the calculations. Additionally,  $\alpha$ -Mn has a unique bcc lattice with 58 atoms in the unit cell,<sup>26</sup> however, for simplicity we modeled it with a plain bcc lattice. The selected Bravais lattice type for each investigated metal is indicated along with the considered surfaces in Figure 1, i.e., (001) for hcp, (110) and (100) for bcc, (100) and (111) for fcc, and (100) for sc metals. In total, we considered 70 different surfaces. The adatoms predominantly adsorb to hollow sites, although for some cases they prefer top or bridge sites: these exceptions are listed in Table S7 in the Supporting Information.

The adatom binding energy ( $E_b$ ), as defined by eq (S4) in the Supporting Information, was calculated for  $(1 \times 1)$  and  $(2 \times 2)$  adatom overlayers, designated as  $E_b^{(1 \times 1)}$  and  $E_b^{(2 \times 2)}$ , respectively. The difference between the two binding energies ( $\Delta E_b$ ):

$$\Delta E_b = E_b^{(1 \times 1)} - E_b^{(2 \times 2)}, \quad (1)$$

was used as the criterion to determine whether lateral interactions are attractive. As to differentiate between attractive (or repulsive) and negligible lateral interactions, we arbitrarily adopt a threshold of 0.1 eV and define interactions to be attractive if  $\Delta E_b < -0.1$  eV, negligible if  $-0.1 \text{ eV} \leq \Delta E_b \leq 0.1 \text{ eV}$ , and repulsive when  $\Delta E_b > 0.1 \text{ eV}$ .

## RESULTS AND DISCUSSION

The main result of this work is shown Figure 2, which schematically presents the type of lateral interactions for the N, O, F, and Cl adatoms on 70 different surfaces of 44 elemental metals. We find that lateral interactions can

be classified into four different groups: (i) the expected repulsive interactions; (ii,iii) the case where the simple ionic model applies and the lateral interactions are either attractive or negligible; and (iv) the case where conditions of the simple ionic model are met, however, surface reconstruction makes the low coverage ( $2 \times 2$ ) overlayer more stable than the high-coverage one. Note that some cases belong to more than one scenario, nevertheless, each specific case is described only by a single category. To this end the following order of precedence is adopted: (1) attractive interactions, (2) reconstruction, and (3) negligible or repulsive interactions. Reconstruction is characterized by metal atoms (ions) nearest to the adatom being substantially displaced toward the adatom thus forming island-like structures on the surface. A typical example is shown in Figure 3.

In order to provide a quantitative measure of the extent of surface reconstruction, we defined the reconstruction quotient ( $f_{\text{rec}}$ ) as:

$$f_{\text{rec}} = A_R/A_{(1 \times 1)}, \quad (2)$$

where  $A_R$  is the area of the reconstructed “cell” and  $A_{(1 \times 1)}$  is the area of the  $(1 \times 1)$  unit-cell (for a schematic definition of these quantities see Figure S3 in the Supporting Information). Because metal ions nearest to the adatom always respond to its presence (by either moving toward or away from it), we define the surface to be reconstructed only when the  $f_{\text{rec}}$  is significantly below 1; we arbitrarily set  $f_{\text{rec}} \leq 0.9$  as the criterion for reconstruction.

In addition to the aforementioned Figure 2, which schematically summarizes the results about lateral interactions,  $E_b$  values for each specific case are tabulated in Tables S1–S6 and plotted along with  $f_{\text{rec}}$  values in Figures S6–S10 in the Supporting Information. In accordance with previous studies,<sup>5–11</sup> our results reveal that repulsion is the dominant case for electronegative adatoms on d-block metal surfaces with few exceptions, such as Fe(100),

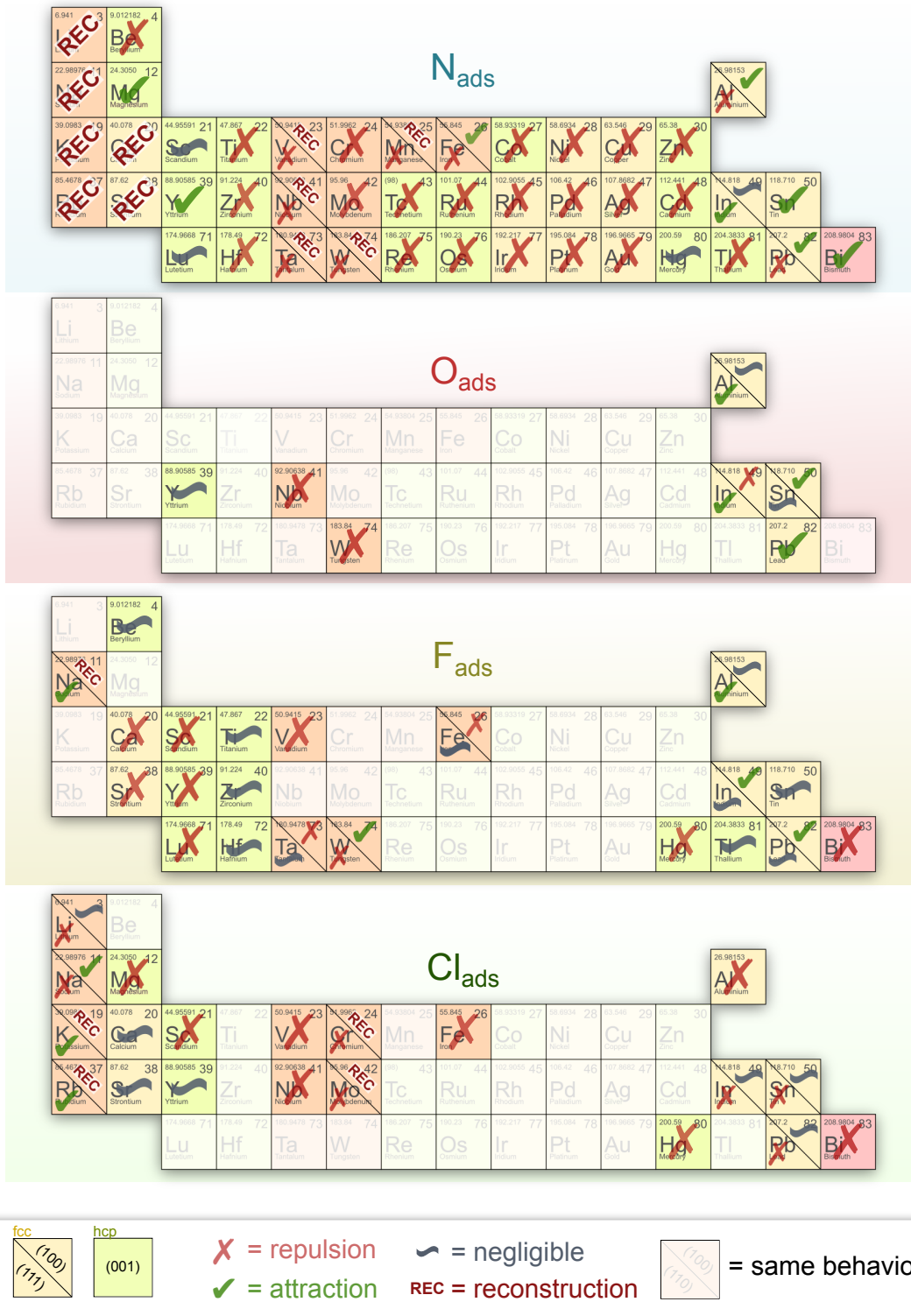


**Figure 2.** A summary of lateral interactions between adatoms on investigated metal surfaces. Four scenarios were found: (i) repulsive interactions, (ii, iii) attractive or negligible interactions, and (iv) reconstruction. For the N adatom all results are explicitly summarized, whereas for other adatoms only differences with respect to the N adatom are shown. For bcc and fcc metals, the results for the two considered surfaces are shown as indicated by the legend.

on which N and O adatoms display attractive interactions, and Hg(001), which displays either attractive, negligible, or repulsive interactions; negligible lateral interactions were

also identified for some adatoms on group 3 and 4 d-block hcp metals. Additionally, reconstruction occurs for (100) surfaces of several bcc d-block metals.

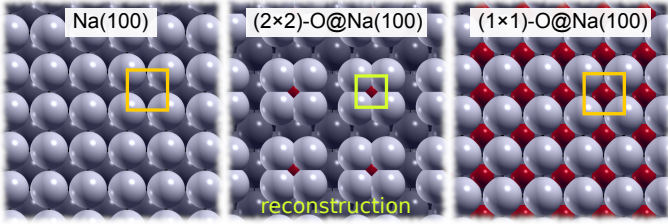


**Figure 3.** An example of surface reconstruction for O on Na(100). For the  $(2 \times 2)$  overlayer the Na atoms closest to the adatom move toward it so that  $\text{Na}_4\text{O}$  islands form. Such reconstruction is not possible for the  $(1 \times 1)$  overlayer due to symmetry. Such a reconstruction occurs for all metals labeled as “REC” in Figure 2, though the extent of reconstruction can vary considerably.

Attractive or negligible lateral interactions are the dominant scenario on the surfaces of p-block metals. In particular N, O, and F display such behavior on a large majority of investigated p-block metal surfaces. Exceptions are repulsive interactions for N on Al(111), Tl(001), and Rb(111); O on In(100) and Tl(001); and F on Bi(100). In contrast, Cl mainly displays repulsive lateral interactions on p-block metal surfaces, with the exception of In(100), Sn(100), and Pb(100) where lateral interactions are negligible.

The third group are the s-block metals where the dominant scenario is reconstruction, in particular for N, O, and to lesser extent for F adatoms. Notable exceptions are Mg and Be, where lateral interactions are attractive and repulsive, respectively. In contrast, for Cl reconstruction occurs only on K(100) and Rb(100), whereas on other surfaces of s-block metals Cl generally displays either attractive or negligible lateral interactions, except on Li(110), Be, Na(110), and Mg where the interactions are repulsive.

Our results indicate that in some cases, such as N, O, and F on alkali metals, where the two conditions of the simple ionic model for the attractive lateral interactions are met (ionic adatom–surface bonding and low height of adatoms), reconstruction occurs instead. This implies that the simple ionic model cannot describe all the situations and needs to be extended, at least conceptually, as to account for the possibility of reconstruction. To this end, we define two quantities termed *unoccupied surface area* ( $A_{\text{usa}}$ ) and *area occupied by the anion* ( $A_{\text{a}}$ ), defined as:

$$A_{\text{usa}} = A_{(1 \times 1)} - \pi R_{\text{c}}^2 \quad \text{and} \quad A_{\text{a}} = \pi R_{\text{a}}^2, \quad (3)$$

where  $A_{(1 \times 1)}$  is the area of the  $(1 \times 1)$  surface cell,  $R_{\text{c}}$  is the ionic radius of the metal cation, calculated as the average of the effective ionic radii for all coordination numbers of the metal in the lowest cationic oxidation state,<sup>27</sup> and  $R_{\text{a}}$  is the effective radius of the anion<sup>27</sup> (for a graphical representation of the *unoccupied surface area*, see Figure S5 in the Supporting Information). The comparison between  $A_{\text{usa}}$  and  $A_{\text{a}}$  is presented in Figure 4. This figure reveals that alkali metals, Ca, and Sr display the largest  $A_{\text{usa}}$  and reconstructions typically occur on their surfaces, in particular for N and O adatoms. Furthermore, it is also evident

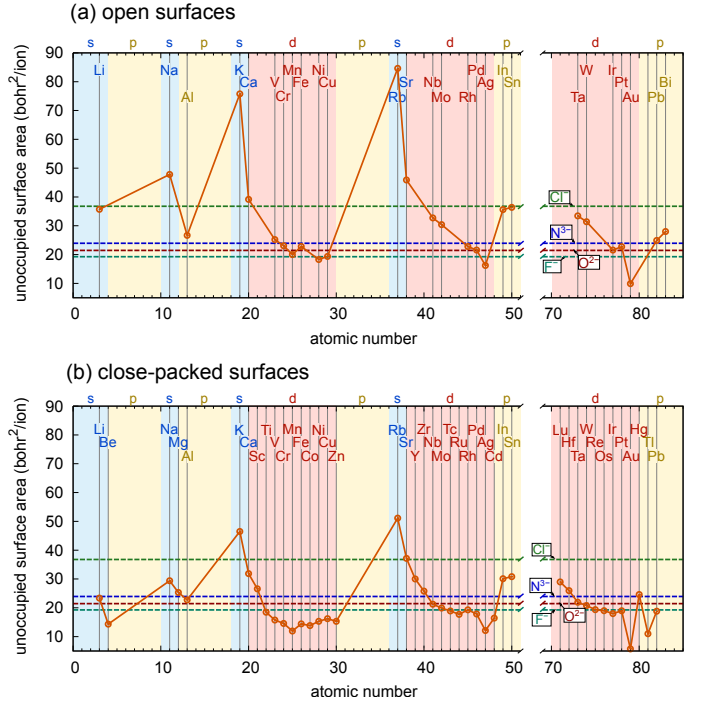


**Figure 4.** Unoccupied surface area ( $A_{\text{usa}}$ ) for (a) open surfaces [fcc(100), bcc(100), and sc(100)] and (b) close-packed surfaces [fcc(111), hcp(001), and bcc(110)]. The horizontal dashed lines indicate the  $A_{\text{a}}$  of adsorbed adatoms, calculated as described in the text.

from the figure that  $A_{\text{a}}$  of  $\text{Cl}^-$  is much larger than  $A_{\text{a}}$  of the other three adatoms and for this reason reconstructions and attractive interactions are considerably less frequent for Cl adatoms (cf. Figure 2). The next relevant observation is that repulsive interactions usually appear when  $A_{\text{usa}}$  is small, i.e., when  $A_{\text{usa}} \lesssim A_{\text{a}}$ . This is the case of transition metal surfaces, where repulsive interactions dominate. Finally, if neither  $A_{\text{usa}} \gg A_{\text{a}}$  nor  $A_{\text{usa}} \lesssim A_{\text{a}}$  applies, then the interactions are likely attractive or negligible. There are, of course, exceptions, because such a simple rule simply cannot encompass all cases.

As a further scrutiny of the utility of the simple ionic model, let us compare the critical height above the surface—i.e., the height above which the simple ionic model predicts that lateral interactions between adatoms are repulsive—with the adatoms heights predicted by DFT calculations (Figure 5). Notably, there is not a single case of attractive lateral interactions with the adatoms located above the critical height. This observation is very reassuring and provides strong support to the validity of our explanation based on the simple ionic model, which differs from the explanations provided by Jacobsen et al.<sup>14</sup> for O on Al(111) and by Cheng et al.<sup>13</sup> for N, O, and F adatoms on Mg(0001). Jacobsen et al.<sup>14</sup> emphasized the role of Al p-states that open new possibilities for hybridization and consequently lead to stronger bonding configurations at high coverage, but this explanation is brought into question by the aforementioned attractive interactions of N, O,



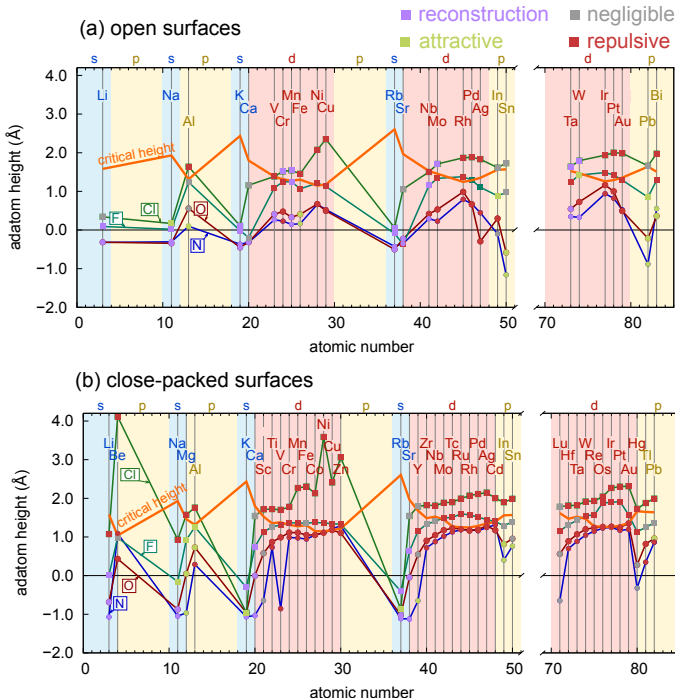


**Figure 5.** Comparison between critical heights as predicted by the simple ionic model and DFT calculated adatom heights for (a) open surfaces [fcc(100), bcc(100), and sc(100)] and (b) close-packed surfaces [fcc(111), hcp(001), and bcc(110)]. Each datapoint is color coded according to the type of interaction as indicated by the legend at the top right.

and F adatoms on Mg(0001),<sup>13</sup> which is an s-metal, as well as by the current findings—among the 24 identified cases of attractive interactions, 11 of them appear on non p-metals (7 on s- and 4 on d-metals, cf. Figure 2). The attractive interactions on Mg are accompanied by an adsorption induced decrease of the work function, which is another anomaly because an increase is typically expected for electronegative adatoms.<sup>28</sup> Cheng et al.<sup>13</sup> attributed both anomalies to a highly polarizable electron spill-out in front of Mg(0001), i.e., the vertical electron charge redistribution (a depletion of charge above the adatom) causes the decrease of the work function,<sup>13,28</sup> whereas attractive interactions were explained by quantum mechanical screening, i.e., a lateral transfer of the spill-out electrons.<sup>13</sup> In contrast, our explanation involves neither the metal p-states nor the highly polarizable electron spill-out, but instead explains the attraction by the simple ionic model—i.e., an interplay of electrostatic and geometric effects—requiring only unpolarizable point ions. It is worth noting that on Mg(0001) the attractive lateral interactions are indeed accompanied by an adsorption induced decrease of the work function, however, the latter is not required for attraction to emerge, as evidenced by Figure S12 in the Supporting Information, which shows the adsorption induced work function change for all currently identified “attraction cases” (whereas Figure S13 shows work function changes for all considered overlayers). Among 24 such cases, the work

function reduces for only 10 of them.

Turning back to Figure 5, its scrutiny for s- and p-block metals reveals that when the adatom height is below the critical height, the lateral interactions are either attractive, negligible, or the surface reconstructs. There are only a few exceptions, i.e., F on Bi(100), O on Tl(001), and N on Tl(001) and Pb(111). The situation is considerably different for transition metals, because for many cases the adatoms are below the critical height, yet the lateral interactions are repulsive. However, transition metals do not fulfill the second requirement of the simple ionic model, that is, the adatom–surface bonding is not sufficiently ionic, due to significant participation of covalent bonding.<sup>9,29–31</sup> Note that transition metals are rather electronegative with work-function values typically above 4 eV<sup>32</sup> (see also Figure S14 in the Supporting Information); exceptions are group-3 metals, which display lower work-functions, but thereon the lateral interactions are usually not predicted by DFT to be repulsive.

Finally, let us focus in more detail on cases denoted as “reconstruction”, where the lower coverage ( $2 \times 2$ ) adatom overlayer is more stable than the high coverage ( $1 \times 1$ ) overlayer. Our analysis indeed reveals that the superior stability of the ( $2 \times 2$ ) overlayer is by and large due to reconstruction, where the metal ions nearest to the adatom move laterally toward it, forming island-like structures on the surface (cf. Figure 3). For example, O on Na(100) displays a  $\Delta E_b$  of 1.8 eV. However, if the larger  $\text{Cl}^-$  ion is adsorbed on Na(100), reconstruction is no longer viable and attractive interactions are found with a  $\Delta E_b$  of  $-0.2$  eV.

The extent to which reconstruction stabilizes the ( $2 \times 2$ ) overlayer of O on Na(100) was estimated by performing a constrained relaxation, where the lateral coordinates of Na atoms in the topmost layer were constrained to their bulk positions. The resulting  $\Delta E_b$  reduces from 1.8 eV for the reconstructed structure to 0.2 eV for the constrained structure, which implies that reconstruction stabilizes the ( $2 \times 2$ ) overlayer by 1.6 eV, which is considerable. Notice, however, that even without reconstruction, the ( $2 \times 2$ ) overlayer remains slightly more stable. The reason for the superiority of the ( $2 \times 2$ ) overlayer can be attributed to the large lattice constant of Na that diminishes the magnitude of electrostatic stabilization (the effect is illustrated in Figure S2 of the Supporting Information). Thus the lack of attractive interactions, even when the top layer is constrained, is likely a consequence of diminished stabilization in combination with other effects, not taken into account by the simple ionic model.

## CONCLUSION

To summarize, by performing DFT calculations of the adsorption of four different electronegative adatoms on 70 surfaces of 44 elemental metals, we showed that even something as conceptually simple as adsorption of electronegative adatoms on metal surfaces, can lead to unanticipated behavior. Understanding such interactions is important

for heterogeneous catalysis and electrochemistry as they may provide a new insight into initial stages of corrosion and passivation. We identified four possible scenarios for the lateral interactions between electronegative adatoms, some of them being unexpected, and explained the reasons why they emerge. Lateral interactions can be: (i) repulsive (this is the expected scenario, but it prevails only on d-block metals), (ii, iii) attractive or negligible (this scenario is predominantly found for p-block metals and Mg; their origin is well explained by our simple ionic model, i.e., attraction is a consequence of predominantly ionic bonding and a low height of adatoms above the surface), or (iv) surface reconstruction of the lower coverage ( $2 \times 2$ ) overlayer provides additional stabilization, making it more stable than the high-coverage ( $1 \times 1$ ) overlayer. This case typically occurs on s-block metals.

## ACKNOWLEDGEMENT

This work has been supported by the Slovenian Research Agency (Grants No. P2-0393).

## References and Notes

[1] Magnussen, O. M. Ordered Anion Adlayers on Metal Electrode Surfaces. *Chem. Rev.* **2002**, *102*, 679–726.

[2] Tripkovic, D. V.; Strmcnik, D.; van der Vliet, D.; Stamenkovic, V.; Markovic, N. M. The role of anions in surface electrochemistry. *Faraday Discuss.* **2009**, *140*, 25–40.

[3] Andryushechkin, B.; Pavlova, T.; Eltsov, K. Adsorption of halogens on metal surfaces. *Surf. Sci. Rep.* **2018**, *73*, 83–115.

[4] Zhu, Q.; Wang, S.-q. Trends and Regularities for Halogen Adsorption on Various Metal Surfaces. *J. Electrochem. Soc.* **2016**, *163*, H796–H808.

[5] Miller, S. D.; Inoglu, N.; Kitchin, J. R. Configurational correlations in the coverage dependent adsorption energies of oxygen atoms on late transition metal fcc(111) surfaces. *J. Chem. Phys.* **2011**, *134*, 104709.

[6] Loffreda, D.; Simon, D.; Sautet, P. Molecular and dissociative chemisorption of NO on palladium and rhodium (100) and (111) surfaces: A density-functional periodic study. *J. Chem. Phys.* **1998**, *108*, 6447–6457.

[7] Gava, P.; Kokalj, A.; de Gironcoli, S.; Baroni, S. Adsorption of chlorine on Ag(111): No subsurface Cl at low coverage. *Phys. Rev. B* **2008**, *78*, 165419.

[8] Ma, S.; Jiao, Z.; Wang, T.; Dai, X. First-principles studies of oxygen chemisorption on Co(0001). *Surf. Sci.* **2014**, *619*, 90–97.

[9] Peljhan, S.; Kokalj, A. Adsorption of Chlorine on Cu(111): A Density-Functional Theory Study. *J. Phys. Chem. C* **2009**, *113*, 14363–14376.

[10] Inderwildi, O. R.; Lebiez, D.; Deutschmann, O.; Warnatz, J. Coverage dependence of oxygen decomposition and surface diffusion on rhodium (111): A DFT study. *J. Chem. Phys.* **2005**, *122*, 034710.

[11] Gossenberger, F.; Roman, T.; Gro, A. Equilibrium coverage of halides on metal electrodes. *Surf. Sci.* **2015**, *631*, 17–22.

[12] Francis, M. F.; Taylor, C. D. First-principles insights into the structure of the incipient magnesium oxide and its instability to decomposition: Oxygen chemisorption to Mg(0001) and thermodynamic stability. *Phys. Rev. B* **2013**, *87*, 075450.

[13] Cheng, S.-T.; Todorova, M.; Freysoldt, C.; Neugebauer, J. Negatively Charged Ions on Mg(0001) Surfaces: Appearance and Origin of Attractive Adsorbate-Adsorbate Interactions. *Phys. Rev. Lett.* **2014**, *113*, 136102.

[14] Jacobsen, J.; Hammer, B.; Jacobsen, K. W.; Nørskov, J. K. Electronic structure, total energies, and STM images of clean and oxygen-covered Al(111). *Phys. Rev. B* **1995**, *52*, 14954–14962.

[15] Kiejna, A.; Lundqvist, B. I. First-principles study of surface and subsurface O structures at Al (111). *Phys. Rev. B* **2001**, *63*, 085405.

[16] Poberžnik, M.; Kokalj, A. Origin of Surprising Attractive Interactions between Electronegative Oxygen Adatoms on Aluminum Surfaces. *J. Phys. Chem. C* **2016**, *120*, 25915–25922.

[17] Giannozzi, P., et al. Advanced capabilities for materials modelling with Quantum ESPRESSO. *J. Phys: Condens. Matter* **2017**, *29*, 465901, Code available from <http://www.quantum-espresso.org/>.

[18] Kokalj, A. **PWTK: PWscf ToolKit**. 2020; Code available from <http://pwtk.ijs.si/>.

[19] Perdew, J. P.; Burke, K.; Ernzerhof, M. Generalized Gradient Approximation Made Simple. *Phys. Rev. Lett.* **1996**, *77*, 3865–3868.

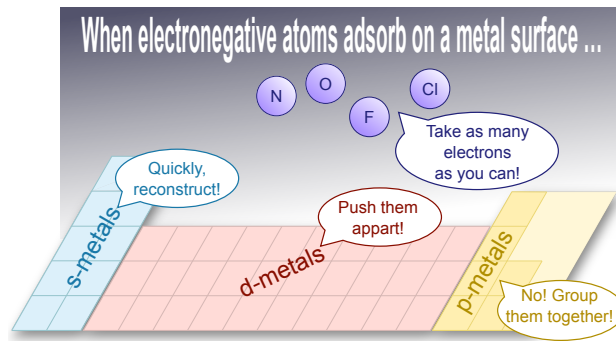
[20] Blöchl, P. E. Projector augmented-wave method. *Phys. Rev. B* **1994**, *50*, 17953–17979.

[21] Dal Corso, A. Pseudopotentials periodic table: From H to Pu. *Comp. Mater. Sci.* **2014**, *95*, 337 – 350.

[22] We used PAW potentials from the **pslibrary** version 1.0.0, except for a few metals potentials from older versions of the **pslibrary** were used, in particular: Na.pbe-spn-kjpaw-ps1.0.2.UPF, Mg.pbe-spn-kjpaw-ps1.0.3.0.UPF, Mn.pbe-spn-kjpaw-ps1.0.2.3.UPF, Tc.pbe-spn-kjpaw-ps1.0.2.3.UPF, W.pbe-spn-kjpaw-ps1.0.2.3.UPF.

- [23] Monkhorst, H. J.; Pack, J. D. Special points for Brillouin zone integrations. *Phys. Rev. B* **1976**, *13*, 5188–5192.
- [24] Methfessel, M.; Paxton, A. T. High-precision sampling for Brillouin-zone integration in metals. *Phys. Rev. B* **1989**, *40*, 3616–3621.
- [25] Kokalj, A. XCrySDen—a new program for displaying crystalline structures and electron densities. *J. Mol. Graph. Model.* **1999**, *17*, 176–179, Code available from <http://www.xcrysdn.org/>.
- [26] Bradley, A. J.; Thewlis, J.; Bragg, W. L. The crystal structure of  $\alpha$ -manganese. *P. R. Soc. Lond. A-Conta.* **1927**, *115*, 456–471.
- [27] Shannon, R. D.; Prewitt, C. T. Revised values of effective ionic radii. *Acta Cryst.* **1970**, *B26*, 1046–1048.
- [28] Michaelides, A.; Hu, P.; Lee, M.-H.; Alavi, A.; King, D. A. Resolution of an Ancient Surface Science Anomaly: Work Function Change Induced by N Adsorption on W{100}. *Phys. Rev. Lett.* **2003**, *90*, 246103.
- [29] Baker, T. A.; Friend, C. M.; Kaxiras, E. Nature of Cl Bonding on the Au(111) Surface: Evidence of a Mainly Covalent Interaction. *J. Am. Chem. Soc.* **2008**, *130*, 3720–3721.
- [30] Migani, A.; Illas, F. A Systematic Study of the Structure and Bonding of Halogens on Low-Index Transition Metal Surfaces. *J. Phys. Chem. B* **2006**, *110*, 11894–11906.
- [31] Roman, T.; Gossenberger, F.; Forster-Tonigold, K.; Groß, A. Halide adsorption on close-packed metal electrodes. *Phys. Chem. Chem. Phys.* **2014**, *16*, 13630–13634.
- [32] Michaelson, H. The work function of the elements and its periodicity. *J. Appl. Phys.* **1977**, *48*, 4729–4733.

## For Table of Contents Only





# Surprising lateral interactions between negatively charged adatoms on metal surfaces

## SUPPORTING INFORMATION

Matic Poberžnik and Anton Kokalj\*

Department of Physical and Organic Chemistry, Jožef Stefan Institute, Jamova 39, SI-1000 Ljubljana, Slovenia

May 1, 2020

ORCID IDs: 0000-0002-4866-4346 (MP), 0000-0001-7237-0041 (AK)

\* Corresponding Author: Anton Kokalj, Tel: +386-1-477-35-23; Fax: +386 1 251 93 85, E-mail: tone.kokalj@ijs.si, URL: <http://www.ijs.si/ijsw/K3-en/Kokalj>

### 1 Description of the simple ionic model

The “simple ionic model” was derived in our previous publication<sup>1</sup> and here we briefly explain its essence. The model is based on the electronic structure analysis of the O/Al(111) system,<sup>1</sup> which reveals that O–Al bonding is ionic and furthermore that the excess electron charge on adatoms mainly comes from the nearest neighbor metal atoms.<sup>1</sup> The last observation is exploited in the simple ionic model, where the adatom gets the electron charge exclusively from the nearest neighbor metal atoms, such that each neighboring metal atom contributes proportionally, as schematically shown in Figure S1. The simple ionic model therefore consists of an ionic bilayer of adatom-anions/metal-cations and can be described by  $N$  ions in the unit-cell at positions  $\{\boldsymbol{\tau}_i\}_{i=1}^N$  and charges  $\{q_i\}_{i=1}^N$ . The interaction energy is then obtained by summing the pairwise Coulomb interactions among the ions in the infinite adatom/metal bilayer, i.e.:

$$E_{\text{int}} = \frac{1}{2} \sum_{\mathbf{R}=\mathbf{0}}^{\infty} \sum_{i,j}^N \frac{q_i q_j}{|\mathbf{R} + \boldsymbol{\tau}_j - \boldsymbol{\tau}_i|} (1 - \delta_{i,j} \delta_{R,0}), \quad (\text{S1})$$

where  $\{\mathbf{R}\}$  are the lattice vectors of a two-dimensional lattice. The role of the  $(1 - \delta_{i,j} \delta_{R,0})$  term is to omit the interaction of an ion with itself ( $i = j$  and

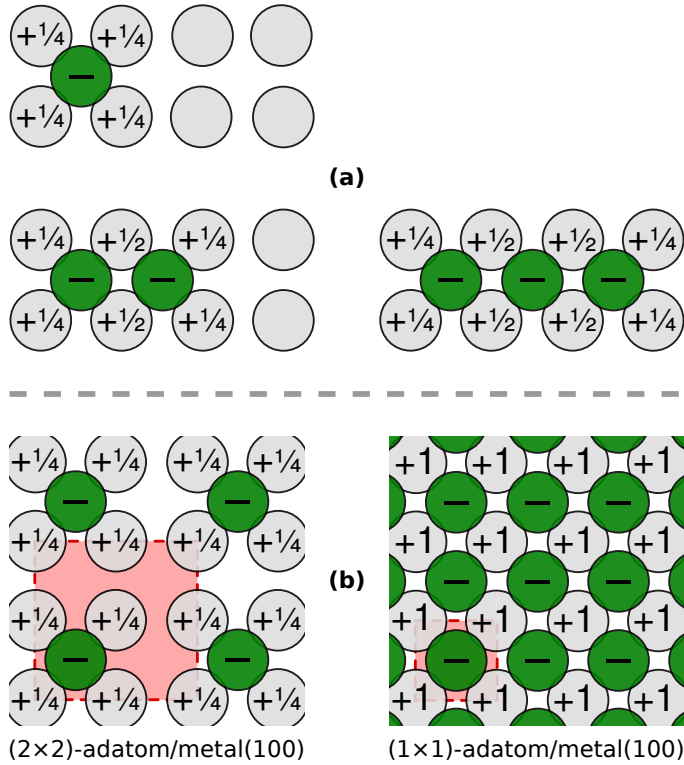
$R = 0$ , where  $R = |\mathbf{R}|$ ). The infinite lattice sum in two-dimensions,  $\sum_{\mathbf{R} \neq \mathbf{0}}^{\infty} (\dots)$ , can be evaluated by explicitly calculating it within the cutoff radius  $R_{\text{cut}}$ , whereas beyond  $R_{\text{cut}}$  it is approximated by an integral, in particular:

$$\begin{aligned} E_{\text{int}} &\simeq \frac{1}{2} \left( \sum_{\mathbf{R}=\mathbf{0}}^{|\mathbf{R}| < R_{\text{cut}}} \sum_{i,j}^N \frac{q_i q_j}{|\mathbf{R} + \boldsymbol{\tau}_j - \boldsymbol{\tau}_i|} (1 - \delta_{i,j} \delta_{R,0}) \right. \\ &\quad \left. + \frac{2\pi}{A} \int_{R_{\text{cut}}}^{\infty} \sum_{i,j}^N \frac{R q_i q_j}{\sqrt{R^2 + (z_j - z_i)^2}} dR \right) \\ &= \frac{1}{2} \left( \sum_{\mathbf{R}=\mathbf{0}}^{|\mathbf{R}| < R_{\text{cut}}} \sum_{i,j}^N \frac{q_i q_j}{|\mathbf{R} + \boldsymbol{\tau}_j - \boldsymbol{\tau}_i|} (1 - \delta_{i,j} \delta_{R,0}) \right. \\ &\quad \left. - \frac{2\pi}{A} \sum_{i,j}^N q_i q_j \sqrt{R_{\text{cut}}^2 + (z_j - z_i)^2} \right), \quad (\text{S2}) \end{aligned}$$

where  $A$  is the area of the unit-cell and  $z_i$  is the  $\hat{z}$ -coordinate of the atomic position  $\boldsymbol{\tau}_i$ , i.e.,  $\boldsymbol{\tau}_i = (x_i, y_i, z_i)$ . Note that due to charge neutrality, the larger is the  $R_{\text{cut}}$ , the smaller is the last sum  $(-\frac{2\pi}{A} \sum_{i,j}^N \dots)$ , due to cancellation between its terms. In particular, the last sum scales as  $(2\pi/A) \mu_z^2 R_{\text{rcut}}^{-1}$ , where  $\mu_z$  is the  $\hat{z}$ -component of the dipole of the ions in the unit-cell,  $\mu_z = \sum_{i=1}^N z_i q_i$ . Hence:

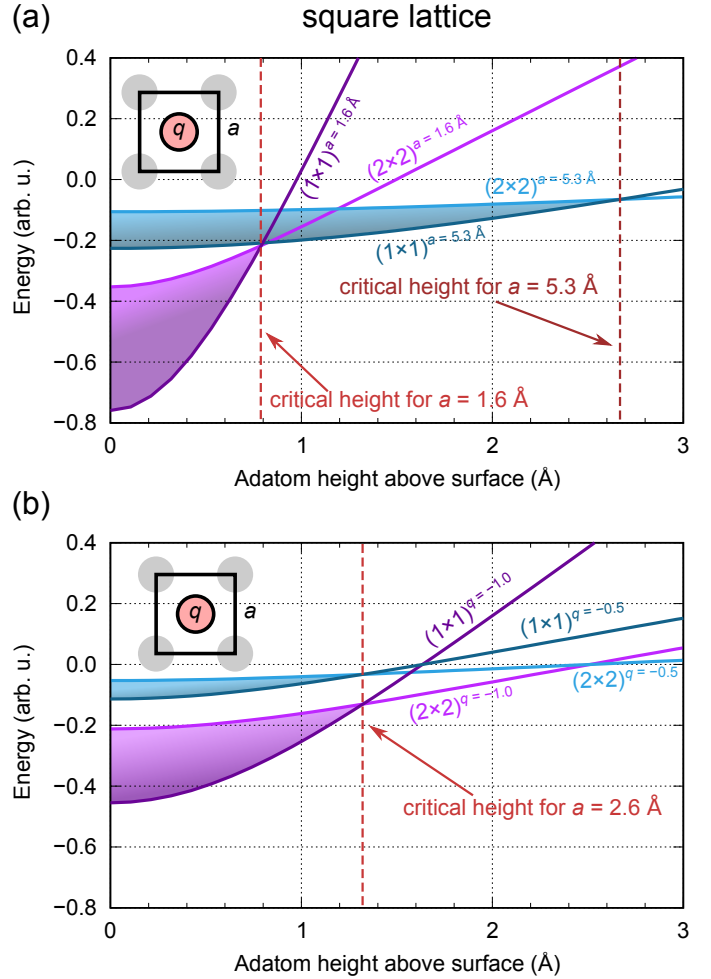
$$- \sum_{i,j}^N q_i q_j \sqrt{R_{\text{cut}}^2 + (z_j - z_i)^2} \simeq \mu_z^2 R_{\text{rcut}}^{-1}. \quad (\text{S3})$$

Figure S2 depicts the results of the simple ionic model for the  $(1 \times 1)$  and  $(2 \times 2)$  adatom overlays over



**Figure S1.** Schematic of the electron charge distribution among adatoms and nearest neighbor metal atoms in the simple ionic model. (a) The charge on adatoms is set to  $q_{\text{ad}}$  (labeled as “-”), whereas the counter-charge is distributed proportionally to the nearest neighbor metal atoms, i.e., for an adatom with  $n$  metal neighbors each of them donates  $q_{\text{ad}}/n$  electrons to the adatom. If a metal atom has no adatom neighbors then it remains charge-neutral, but if it has  $m$  adatom neighbors then it donates  $q_{\text{ad}}/n$  electrons to each, thus in total  $mq_{\text{ad}}/n$  to all of them. (b) Charge distribution for (2×2) and (1×1) adatom overlayers on a square lattice of metal atoms, which is compatible with bcc(100), fcc(100), and sc(100). Unit-cells are indicated in red.

a square lattice of metal atoms, with the interaction energy shown as a function of adatom height above the surface. The figure illustrates the dependence of the interaction energy on the lattice parameter (Figure S2a) and on the adatom charge (Figure S2b). The most important result of the ionic model is that there exist a critical adatom height below which the high-coverage (1×1) overlayer is more stable than the low coverage overlayers (currently only the (2×2) overlayer is considered for low coverage, but in our previous work<sup>1</sup> we considered even lower coverages). This effect is referred to as “stabilization” in the following.



**Figure S2.** The prediction of the simple ionic model for the (1×1) and (2×2) adatom overlayers above a square lattice of metal atoms, which is compatible with the bcc(100), fcc(100), and sc(100) surfaces. Notice that below the critical height the high-coverage (1×1) overlayer is more stable than the lower-coverage (2×2) overlayer. (a) The dependence of the interaction energy and the critical height on the lattice parameter for  $a = 1.6 \text{ \AA}$  and  $a = 5.3 \text{ \AA}$ . Notice that the (1×1) over (2×2) preference below the critical height decreases by increasing the lattice parameter, while concomitantly the critical height becomes larger. (b) The dependence of the interaction energy on the charge of the adatom for  $q = -0.5$  and  $q = -1.0$ . Because the energy depends quadratically on the charge, the (1×1) over (2×2) preference below the critical height decreases with a decrease in charge magnitude.

The critical height obviously depends on the lattice parameter due to geometric reasons, i.e., the larger is the lattice parameter, the larger is the critical height.

Concomitantly with the increase of the lattice parameter the extent of stabilization obviously decreases (Figure S2a). As for the dependence on the adatom charge, the stabilization obviously increases with the magnitude of the adatom charge (Figure S2b), because the energy depends quadratically on the charge. Some of these dependencies can be easily understood from eq (S1).

## 2 Definitions

### 2.1 Binding energy

DFT calculated binding energies were calculated as:

$$E_b = E_{X/\text{slab}} - E_X - E_{\text{slab}}, \quad (\text{S4})$$

where  $X$  stands for the adatom (either N, O, F, or Cl) and  $E_{X/\text{slab}}$ ,  $E_X$ , and  $E_{\text{slab}}$  are the total energies of the adatom-slab system, standalone adatom, and bare slab, respectively. The binding energies for bcc, fcc, and hcp adatom/metal systems are plotted in Figures S6 to S10 and tabulated in Tables S1 to S5. The  $E_b$  values of sc (simple-cubic) systems are given in Table S6, but they are not plotted, because only Bi is “considered” to crystallize in this lattice type. Note that Bi and some other investigated metals crystallize in more “exotic” lattices, however, in order to simplify the calculations, they were modeled by one among the bcc, fcc, hcp, or sc lattice types, as described in the main text.

### 2.2 Reconstruction quotient

In addition to attractive and repulsive lateral interactions we also identified another possibility, when the two conditions of the simple ionic model for the attractive lateral interactions are met (ionic adatom–surface bonding and low height of adatoms). In particular, surface reconstruction stabilizes the  $(2 \times 2)$  overlayer and makes it more stable than the  $(1 \times 1)$  overlayer. In order to quantify the extent of reconstruction for each adatom/metal pair, we defined the reconstruction quotient ( $f_{\text{rec}}$ ) by eq (2) in the main text. The way the reconstruction quotient is calculated is schematically illustrated in Figure S3. We defined the surface to be reconstructed only when  $f_{\text{rec}}$  is significantly below 1; we arbitrarily set  $f_{\text{rec}} \leq 0.9$  as the criterion for reconstruction.

We should comment on how the reconstruction quotient was calculated for close-packed bcc(110), fcc(111), and hcp(001) surfaces. In particular, on

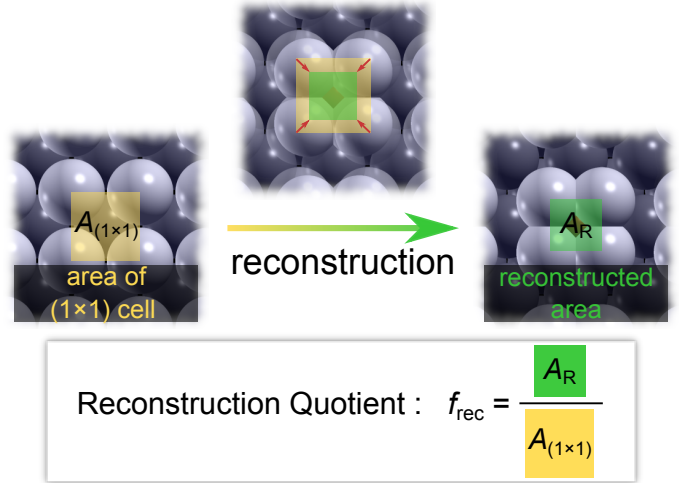


**Figure S3.** A schematic definition of the reconstruction quotient,  $f_{\text{rec}} = A_R/A_{(1 \times 1)}$ .  $A_{(1 \times 1)}$  is the area of the  $(1 \times 1)$  unit-cell (left panel), whereas  $A_R$  is the area enclosed by the four metal atoms nearest to the adatom forming a  $(2 \times 2)$  overlayer (right panel). The reconstruction quotient was used to estimate the degree of reconstruction, in particular, we used  $f_{\text{rec}} \leq 0.9$  as the criterion for reconstruction.

bcc(110) the adatoms were found in two distinct sites, i.e., three-fold and four-fold hollow sites (see Figure S4), whereas on fcc(111) and hcp(001) both fcc- and hcp-hollow sites are three-fold coordinated. For all the three-fold hollow sites,  $f_{\text{rec}}$  was estimated by considering the area spanned by the three metal cations nearest to the adatom, whereas for the bcc(110) four-fold hollow site the area spanned by the four nearest metal cations was taken into account.

The obtained values for the reconstruction quotient are plotted on the right-hand side of Figures S6 to S10. The plots clearly show that the extent of reconstruction is the greatest for N and O adatoms on bcc(100) surfaces, where alkali metals stand out the most. In the case of fcc metals reconstruction occurs for N and O on the surfaces of Ca and Sr. According to the  $f_{\text{rec}}$  value reconstruction also occurs for N on Sn(100), however, since the  $(1 \times 1)$  overlayer is still more stable this case is labeled as “attraction” in the main text.

### 2.3 Unoccupied surface area

As an approximate *ad hoc* criterion for which adatom/metal pairs reconstruction can be expected, we defined a quantity termed *unoccupied surface area*,

whose calculation is schematically illustrated in Figure S5.

### 3 Stability of adsorption sites

The adatoms were mainly adsorbed in hollow sites; for fcc(111) predominantly fcc-hollow and for hcp(001) both fcc- and hcp-hollow sites were considered. However, for a few specific cases hollow sites are either unstable or less stable than bridge or top sites. The cases where non-hollow sites (or also hcp sites for fcc(111)) were found to be the stablest are listed in Table S7. We begin our analysis by noticing that our results are in line with those reported by Zhu et al.<sup>2</sup> for halogen adatoms (see the comparison in Figure S11). Namely, both F and Cl prefer the top site on Al(111) at the lower coverage. The top site is also the preferred site for F on Ir(111) and Pt(111), whereas for Cl on Ir(111) both fcc and top sites display similar stabilities. Additionally, on Ca(111) and Sr(111) the hcp site is found to be more stable than the fcc site for O, F, and Cl, irrespective of the coverage. Note that most of these exceptions have been reported by other authors as well.<sup>3</sup> As for bcc metals the top site is preferred for F on W(110). However, we find that F prefers the hollow site on Mo(110) and not the top site as reported by Zhu et al.<sup>2</sup> The site preference for F and Cl on hcp metals is also reproduced, the only difference is that according to our calculations Cl prefers the fcc site on Tc(001), whereas Zhu et al. reported that the hcp site is more stable. Both sets of calculations, however, show that the two sites have very similar stabilities. The calculated  $E_b$  values for  $(2 \times 2)$  layers of F and Cl are compared to those reported by Zhu et al. in Figure S11. For Cl the average difference between the two sets of  $E_b$  values is  $-0.10 \pm 0.09$  eV, whereas for F the average difference is  $0.19 \pm 0.15$  eV.

In addition to the already documented site anomalies, we found that F prefers to adsorb on the top site of Os(001) and bridge site of Ru(001), whereas the top site is the most stable for Cl on Fe(110), for Cl on Mn(110) at high coverage, and for F on Bi(100). For O and F on Al(100) and Fe(100) the bridge site is also the more stable site at low coverage, whereas at high coverage the two sites generally display similar stabilities. For Cl on Al(100) and Fe(100) the bridge site is favored for both investigated coverages.

Finally, as mentioned above adatoms adsorbed on hollow sites of bcc(110) surfaces display two specific

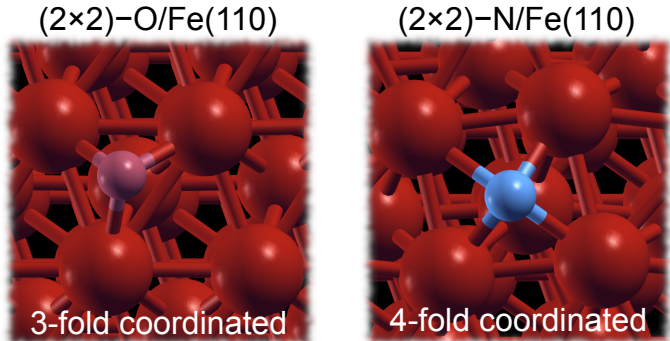


**Figure S4.** Three- and four-fold hollow sites on the bcc(110) surfaces. As an example, the  $(2 \times 2)$  overlayer of O on Fe(110) displays three-fold, whereas the  $(2 \times 2)$  overlayer of N on Fe(110) displays four-fold coordination.

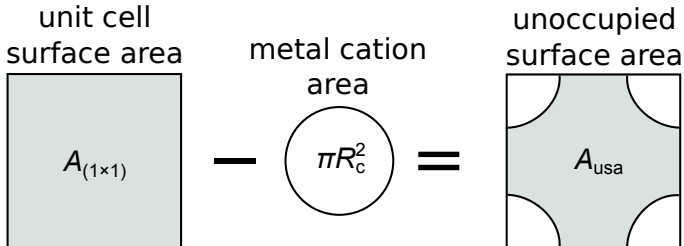


**Figure S5.** The *unoccupied* surface area is calculated by subtracting the area occupied by the metal cation from the area of the  $(1 \times 1)$  unit-cell. For the radius of the metal cation,  $R_c$ , the average value of cationic radii for all coordination numbers of the lowest cationic oxidation state is used. Radii were taken from Shannon and Prewitt.<sup>4</sup>

configurations, one where the adatom is three-fold coordinated and a second one, where the adatom is four-fold coordinated. Adatoms adsorb predominantly in the three-fold hollow site, the exceptions are N on Li, Na, K, V, Cr, Fe; O on Li and Na; and Cl on Li, Na, and Fe. An example of three-fold and four-fold hollow sites on bcc(110) is shown in Figure S4.

### 4 Adsorption induced work function changes

In some cases, such as N, O, and F adatoms on Mg(0001) the lateral attractive interaction between adatoms are accompanied by an adsorption induced decrease of the work function.<sup>5</sup> It should be noted, however, that decrease of the work function is not required for attraction to emerge, as evidenced by Figure S12, which shows the adsorption induced work function change for all the “attraction cases” cur-

rently identified. Among 24 such identified cases, work function reduces for only 10 of them.

Figure S13 plots the adsorption induced work function changes for all the considered adatom overlayers and Figure S14 shows the experimental work functions for either closed-packed or polycrystalline surfaces of the 44 metals considered in this study.

## References

- [1] Poberžnik, M.; Kokalj, A. Origin of Surprising Attractive Interactions between Electronegative Oxygen Adatoms on Aluminum Surfaces. *J. Phys. Chem. C* **2016**, *120*, 25915–25922.
- [2] Zhu, Q.; Wang, S.-q. Trends and Regularities for Halogen Adsorption on Various Metal Surfaces. *J. Electrochem. Soc.* **2016**, *163*, H796–H808.
- [3] Roman, T.; Gossenberger, F.; Forster-Tonigold, K.; Groß, A. Halide adsorption on close-packed metal electrodes. *Phys. Chem. Chem. Phys.* **2014**, *16*, 13630–13634.
- [4] Shannon, R. D.; Prewitt, C. T. Revised values of effective ionic radii. *Acta Cryst.* **1970**, *B26*, 1046–1048.
- [5] Cheng, S.-T.; Todorova, M.; Freysoldt, C.; Neugebauer, J. Negatively Charged Ions on Mg(0001) Surfaces: Appearance and Origin of Attractive Adsorbate-Adsorbate Interactions. *Phys. Rev. Lett.* **2014**, *113*, 136102.
- [6] Lide, D. R., Ed. *CRC Handbook of Chemistry and Physics*, 85th ed.; CRC Press: Boca Raton, Florida USA, 2005.



**TABLE S1:** Binding energies for  $(1 \times 1)$  and  $(2 \times 2)$  overlayers of the four considered adatoms adsorbed on hollow sites of the bcc(100) metal surfaces. All values are in eV/adatom.

Surface	$N_{\text{ads}}$		$O_{\text{ads}}$		$F_{\text{ads}}$		$Cl_{\text{ads}}$	
	$(2 \times 2)$	$(1 \times 1)$	$(2 \times 2)$	$(1 \times 1)$	$(2 \times 2)$	$(1 \times 1)$	$(2 \times 2)$	$(1 \times 1)$
Li(100)	-6.25	-3.37	-8.27	-5.89	-6.52	-6.36	-5.20	-5.26
Na(100)	-3.96	-1.93	-6.24	-4.38	-5.90	-5.62	-4.86	-5.03
K(100)	-3.54	-1.32	-6.07	-3.85	-5.96	-5.43	-5.15	-5.05
V(100)	-8.48	-8.11	-8.16	-7.81	-5.18	-4.87	-4.58	-3.84
Cr(100)	-8.23	-7.44	-7.59	-6.71	-4.56	-4.39	-4.75	-3.20
Mn(100)	-7.57	-6.74	-7.22	-5.72	-4.99	-3.97	-4.87	-2.67
Fe(100)	-5.82	-6.27	-5.25 <sup>a</sup>	-5.64	-5.31 <sup>a</sup>	-4.46 <sup>a</sup>	-3.42 <sup>a</sup>	-3.20 <sup>a</sup>
Rb(100)	-3.36	-1.17	-5.90	-3.70	-5.97	-5.34	-5.14	-4.97
Nb(100)	-8.24	-7.75	-7.75	-7.31	-5.00	-4.77	-4.51	-4.09
Mo(100)	-7.56	-6.99	-6.83	-6.02	-4.27	-4.15	-4.60	-3.51
Ta(100)	-8.32	-7.72	-7.64	-6.99	-4.76	-4.54	-4.31	-3.85
W(100)	-7.73	-6.74	-6.66	-5.58	-3.88	-4.03	-4.47	-3.44

<sup>a</sup> The reported value is for the more stable bridge site.

**TABLE S2:** As in Table S1, but for hollow sites on the bcc(110) surfaces. All values are in eV/adatom.

Surface	$N_{\text{ads}}$		$O_{\text{ads}}$		$F_{\text{ads}}$		$Cl_{\text{ads}}$	
	$(2 \times 2)$	$(1 \times 1)$	$(2 \times 2)$	$(1 \times 1)$	$(2 \times 2)$	$(1 \times 1)$	$(2 \times 2)$	$(1 \times 1)$
Li(110)	-6.71	-5.61	-8.44	-7.84	-6.76	-6.77	-5.21	-3.75
Na(110)	-3.94	-3.26	-6.32	-6.07	-5.96	-6.17	-4.83	-4.15
K(110)	-3.52	-2.62	-6.00	-5.42	-6.13	-6.12	-5.03	-5.16
V(110)	-7.82	-6.41	-8.05	-7.15	-5.90	-5.71	-4.88	-2.90
Cr(110)	-7.25	-5.55	-7.47	-6.45	-5.21	-4.76	-4.44	-1.52
Mn(110)	-6.95	-5.38	-7.17	-6.02	-4.98	-4.13	-4.53	-1.22 <sup>a</sup>
Fe(110)	-6.27	-5.06	-5.96	-5.62	-4.01	-4.00	-3.76 <sup>a</sup>	-1.57 <sup>a</sup>
Rb(110)	-3.09	-2.40	-5.96	-5.14	-6.08	-6.03	-5.02	-5.17
Nb(110)	-7.19	-6.66	-7.69	-7.20	-5.70	-5.67	-4.79	-3.90
Mo(110)	-7.00	-5.89	-7.21	-6.67	-5.04	-4.79	-4.36	-2.85
Ta(110)	-7.68	-7.10	-8.02	-7.54	-5.67	-5.68	-4.79	-3.95
W(110)	-7.15	-6.13	-7.19	-6.87	-5.15 <sup>a</sup>	-4.87 <sup>a</sup>	-4.12	-2.78

<sup>a</sup> The reported value is for the more stable top site.

## (100) surfaces of bcc metals

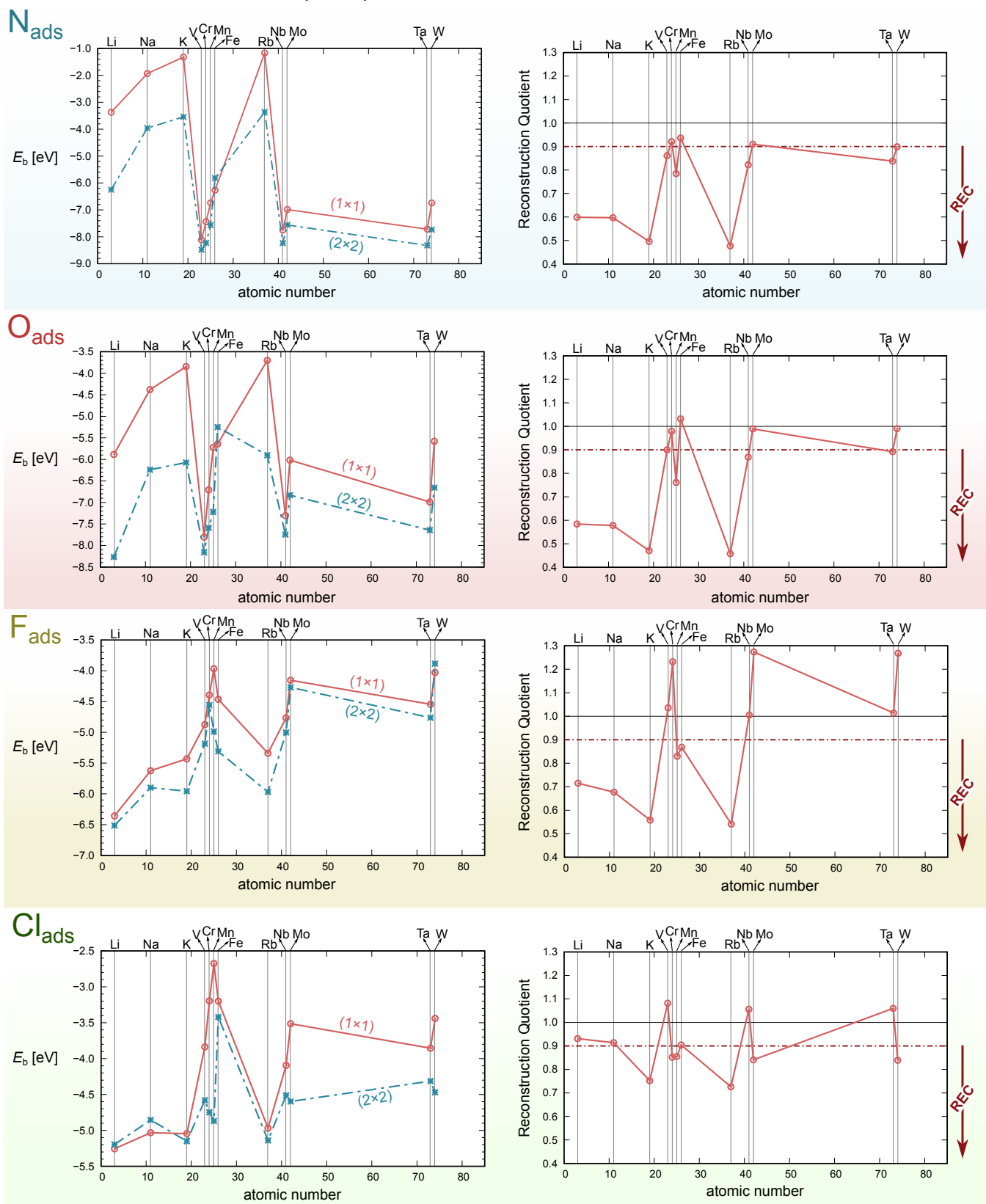


**Figure S6.** Left: binding energies ( $E_b$ ) of adatoms on bcc(100) surfaces for (1 × 1) and (2 × 2) overlayers. Right: the degree of reconstruction, expressed in terms of the reconstruction quotient ( $f_{\text{rec}}$ ). The red dash-dotted line at  $f_{\text{rec}} = 0.9$  indicates the adopted threshold for the reconstruction. Lines are drawn to guide the eye.

# (110) surfaces of bcc metals

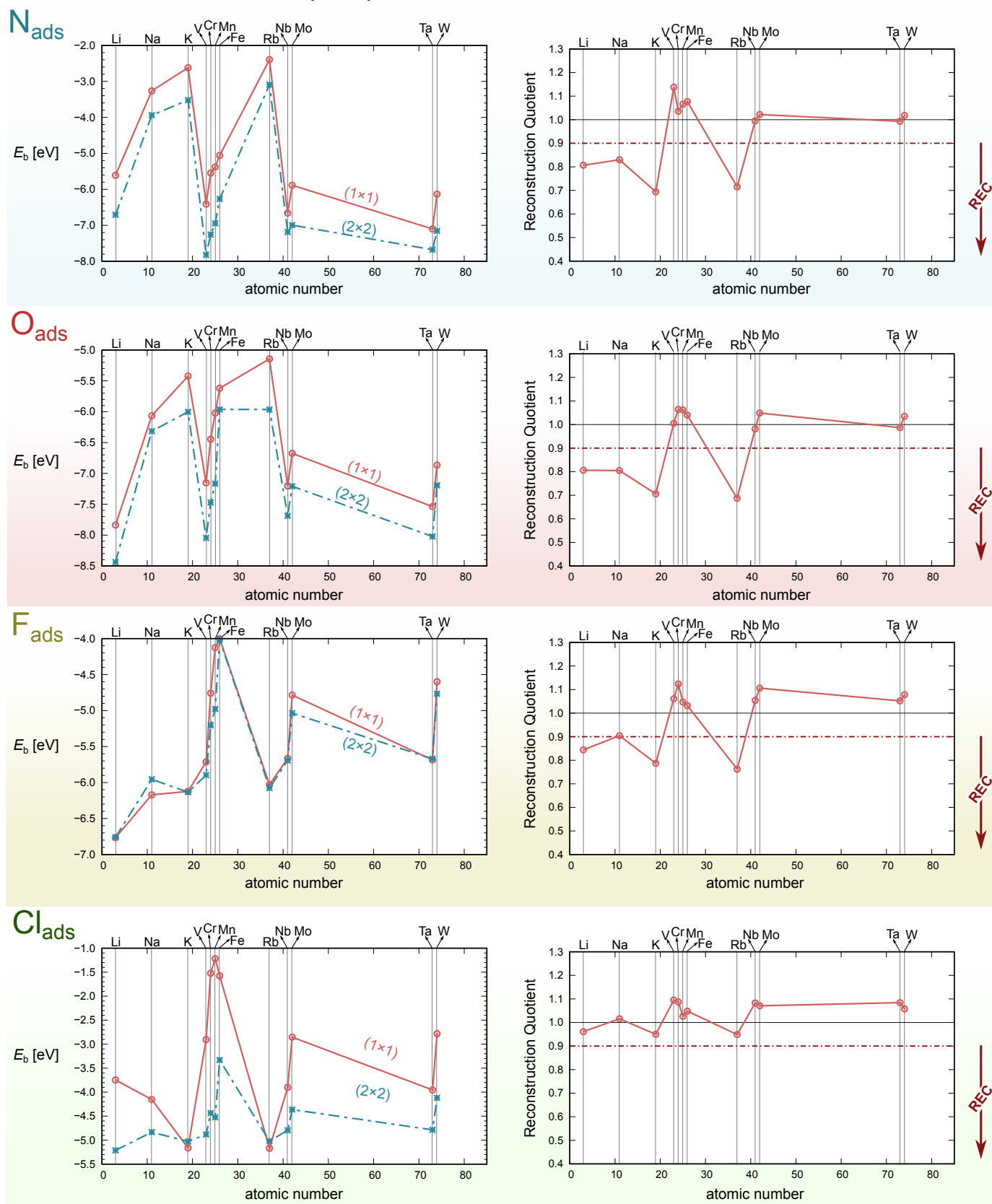


Figure S7. As in Figure S6, but for bcc(110) surfaces.

# (100) surfaces of fcc metals

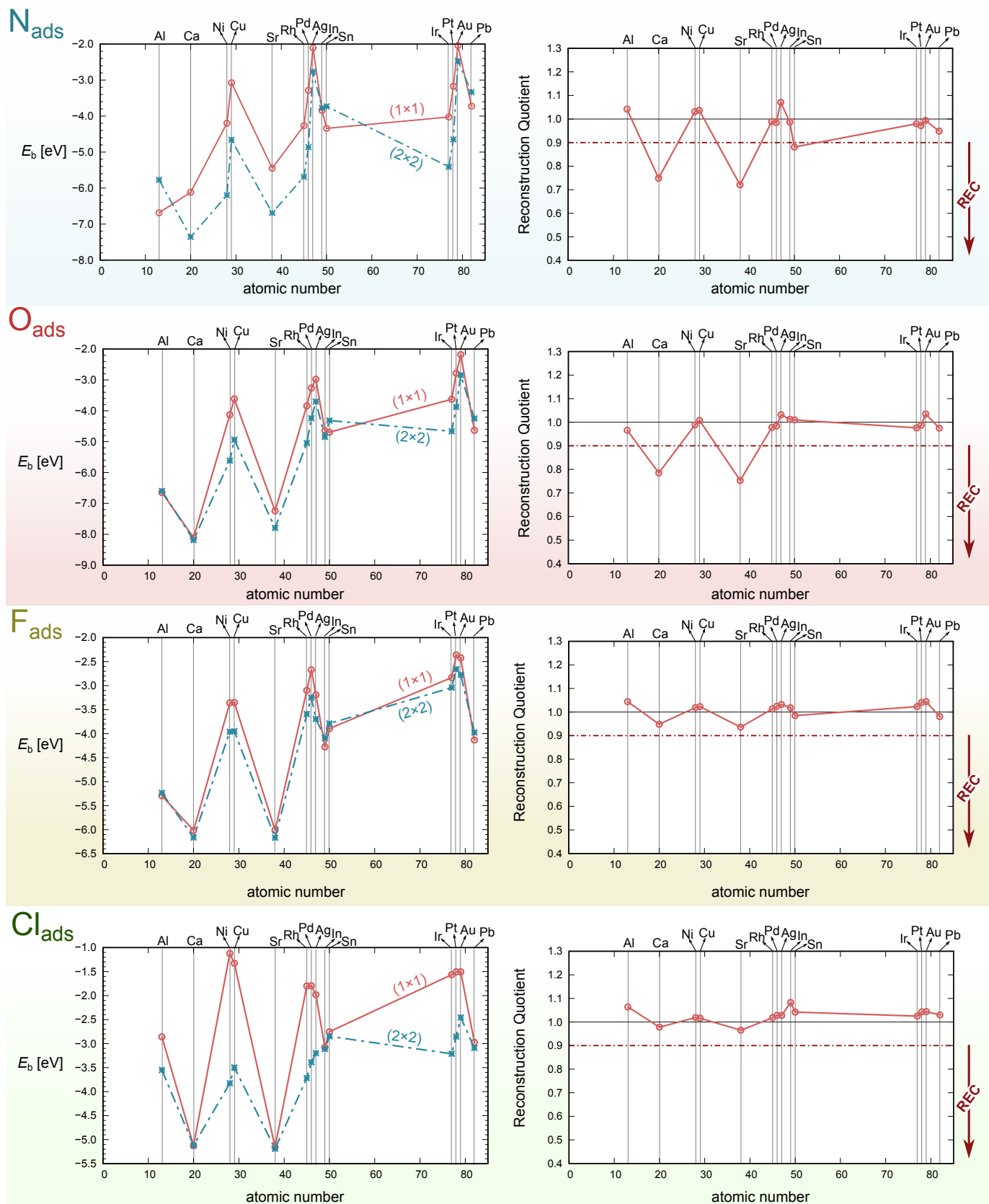


Figure S8. As in Figure S6, but for fcc(100) surfaces.

# (111) surfaces of fcc metals

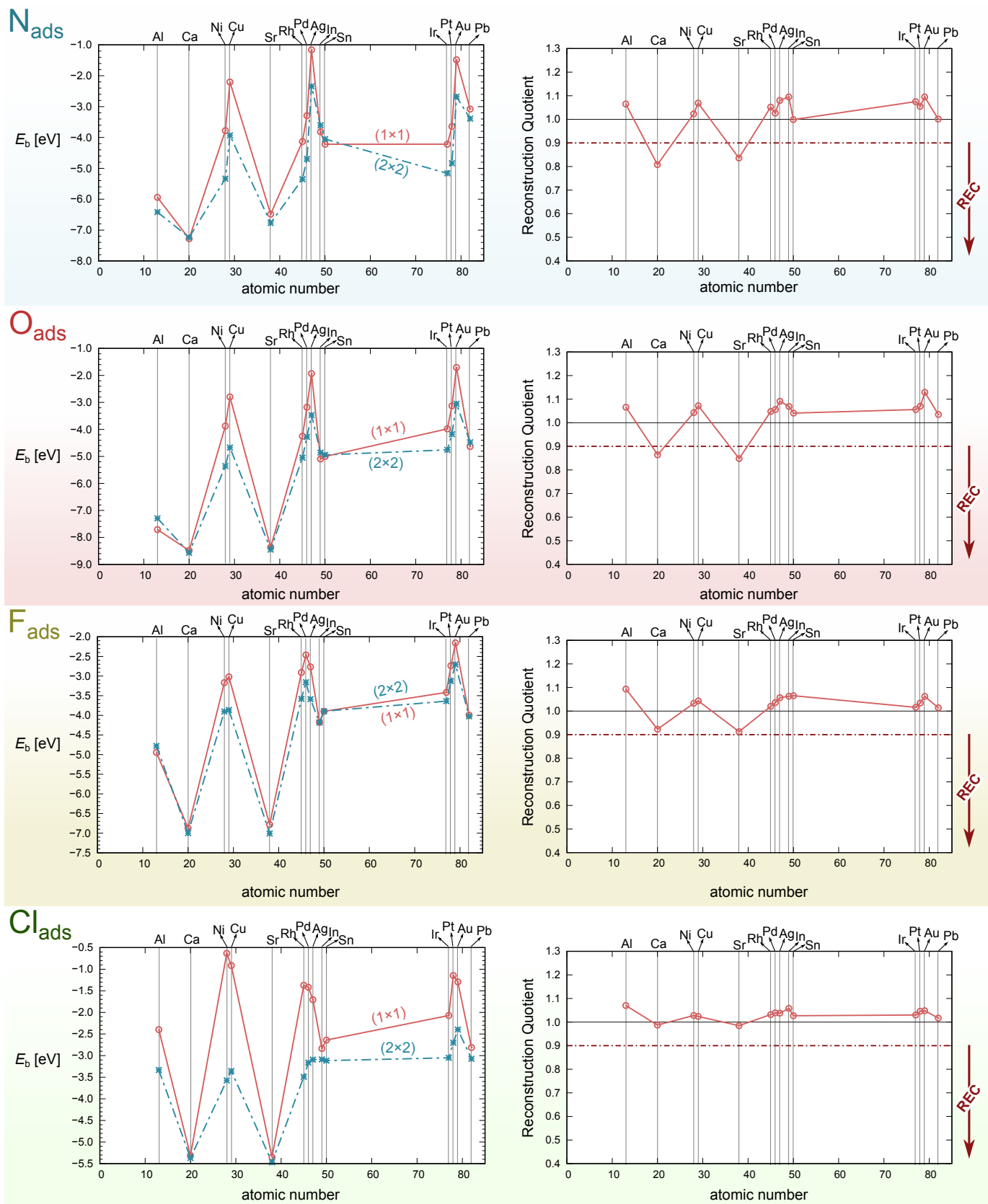
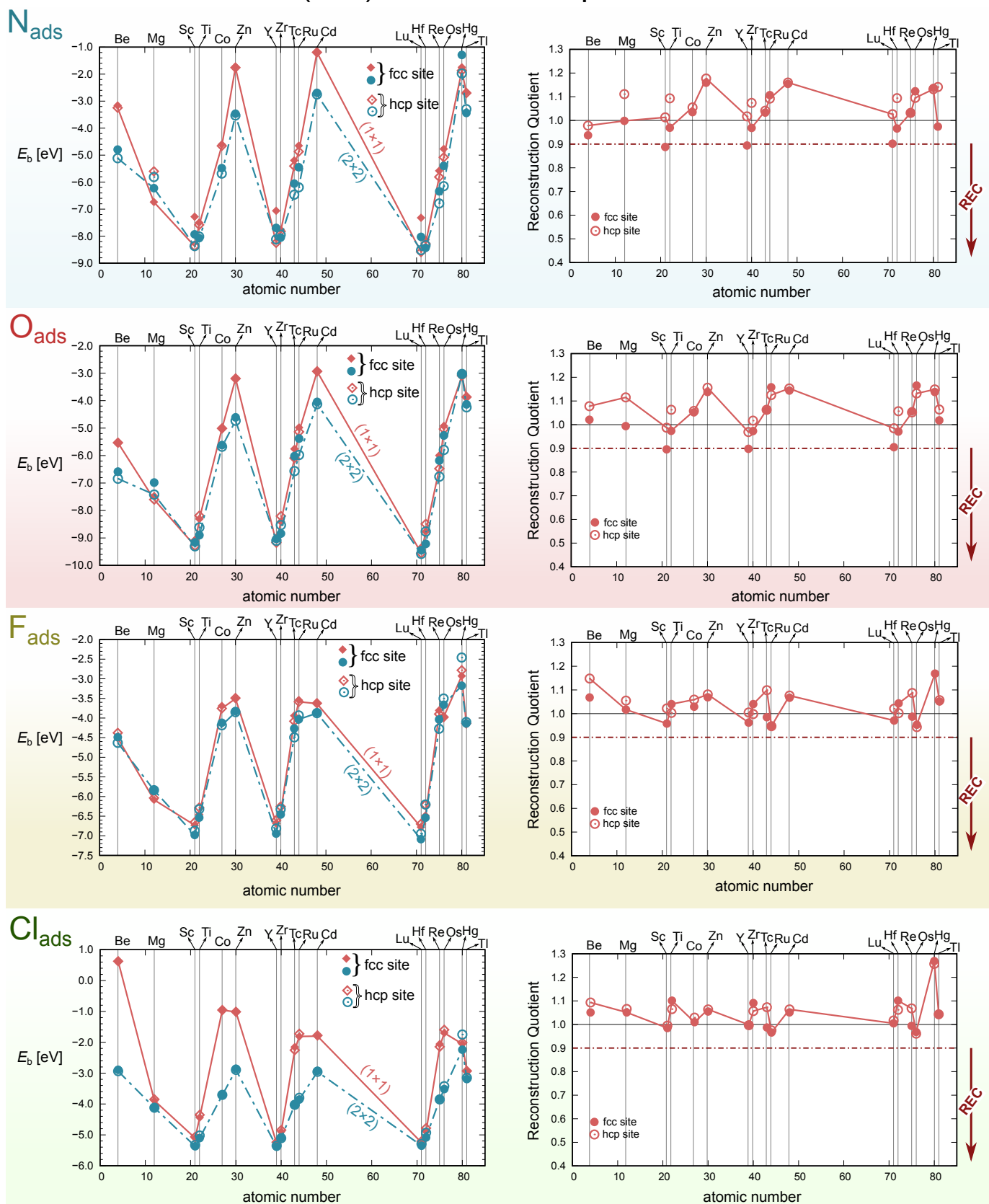


Figure S9. As in Figure S6, but for fcc(111) surfaces.



## (001) surfaces of hcp metals



**Figure S10.** As in Figure S6, but for hcp(001) surfaces. Filled and empty symbols designate the fcc and hcp sites, respectively. The lines connect the most stable of the two considered sites and are drawn to guide the eye.

**TABLE S3:** As in Table S1, but for fcc sites on the fcc(111) surfaces. All values are in eV/adatom.

Surface	N <sub>ads</sub>		O <sub>ads</sub>		F <sub>ads</sub>		Cl <sub>ads</sub>	
	(2 × 2)	(1 × 1)	(2 × 2)	(1 × 1)	(2 × 2)	(1 × 1)	(2 × 2)	(1 × 1)
Al(111)	-6.42	-5.94	-7.29	-7.71	-5.05 <sup>a</sup>	-4.95	-3.52 <sup>a</sup>	-2.40
Ca(111)	-7.24	-7.28	-8.57 <sup>b</sup>	-8.48 <sup>b</sup>	-7.00 <sup>b</sup>	-6.87 <sup>b</sup>	-5.37 <sup>b</sup>	-5.31 <sup>b</sup>
Ni(111)	-5.33	-3.78	-5.36	-3.87	-3.90	-3.17	-3.57	-0.63
Cu(111)	-3.93	-2.20	-4.67	-2.80	-3.86	-3.02	-3.36	-0.91
Sr(111)	-6.77 <sup>b</sup>	-6.48	-8.45 <sup>b</sup>	-8.36 <sup>b</sup>	-7.00 <sup>b</sup>	-6.78 <sup>b</sup>	-5.47 <sup>b</sup>	-5.35 <sup>b</sup>
Rh(111)	-5.35	-4.13	-5.05	-4.25	-3.58	-2.91	-3.49	-1.37
Pd(111)	-4.69	-3.29	-4.28	-3.18	-3.16	-2.46	-3.16	-1.42
Ag(111)	-2.34	-1.16	-3.47	-1.93	-3.59	-2.77	-3.09	-1.71
In(111)	-3.61	-3.82	-4.86	-5.09	-4.18	-4.18	-3.09	-2.83
Sn(111)	-4.05	-4.22	-4.94	-5.00	-3.90	-3.90	-3.12	-2.64
Ir(111)	-5.16	-4.22	-4.76	-3.98	-3.46 <sup>a</sup>	-3.42 <sup>a</sup>	-3.05 <sup>a</sup>	-2.07
Pt(111)	-4.83	-3.65	-4.18	-3.13	-3.13 <sup>a</sup>	-2.74 <sup>a</sup>	-2.70	-1.15
Au(111)	-2.68	-1.48	-3.05	-1.71	-2.71	-2.15	-2.40	-1.29
Pb(111)	-3.39	-3.08	-4.48	-4.63	-4.03	-4.00	-3.07	-2.81

<sup>a</sup> The reported value is for the more stable top site.<sup>b</sup> The reported value is for the more stable hcp site.**TABLE S4:** As in Table S1, but for hollow sites on the fcc(100) surfaces. All values are in eV/adatom.

Surface	N <sub>ads</sub>		O <sub>ads</sub>		F <sub>ads</sub>		Cl <sub>ads</sub>	
	(2 × 2)	(1 × 1)	(2 × 2)	(1 × 1)	(2 × 2)	(1 × 1)	(2 × 2)	(1 × 1)
Al(100)	-5.77	-6.69	-6.60 <sup>a</sup>	-6.65	-5.23 <sup>a</sup>	-5.29	-3.55 <sup>a</sup>	-2.86 <sup>a</sup>
Ca(100)	-7.36	-6.12	-8.19	-8.11	-6.16	-6.02	-5.12	-5.12
Ni(100)	-6.20	-4.20	-5.61	-4.13	-3.96	-3.36	-3.83	-1.12
Cu(100)	-4.66	-3.07	-4.94	-3.61	-3.95	-3.35	-3.50	-1.33
Sr(100)	-6.69	-5.45	-7.80	-7.24	-6.17	-6.01	-5.19	-5.16
Rh(100)	-5.69	-4.26	-5.04	-3.84	-3.59	-3.10	-3.71	-1.80
Pd(100)	-4.86	-3.29	-4.24	-3.26	-3.25	-2.67	-3.39	-1.79
Ag(100)	-2.77	-2.10	-3.70	-2.98	-3.69	-3.19	-3.20	-1.98
In(100)	-3.77	-3.84	-4.85	-4.64	-4.09	-4.28	-3.11	-3.08
Sn(100)	-3.73	-4.34	-4.32	-4.69	-3.79	-3.89	-2.85	-2.75
Ir(100)	-5.41	-4.03	-4.66	-3.62	-3.04	-2.83	-3.21	-1.56
Pt(100)	-4.65	-3.17	-3.87	-2.78	-2.65	-2.36	-2.85	-1.50
Au(100)	-2.47	-2.04	-2.84	-2.18	-2.77	-2.42	-2.46	-1.51
Pb(100)	-3.34	-3.73	-4.25	-4.63	-3.98	-4.13	-3.09	-2.97

<sup>a</sup> The reported value is for the more stable bridge site.

**TABLE S5:** As in Table S1, but for fcc and hcp sites on the hcp(001) surfaces. The most stable site is emphasized in bold for each particular case. All values are in eV/adatom.

Surface	N <sub>ads</sub>		O <sub>ads</sub>		F <sub>ads</sub>		Cl <sub>ads</sub>	
	(2 × 2)	(1 × 1)	(2 × 2)	(1 × 1)	(2 × 2)	(1 × 1)	(2 × 2)	(1 × 1)
	fcc/hcp	fcc/hcp	fcc/hcp	fcc/hcp	fcc/hcp	fcc/hcp	fcc/hcp	fcc/hcp
Be(001)	-4.79/- <b>5.12</b>	-3.16/- <b>3.25</b>	-6.59/- <b>6.84</b>	-5.51/- <b>5.53</b>	-4.49/- <b>4.63</b>	- <b>4.51</b> /-4.38	-2.89/- <b>2.94</b>	+ <b>0.63</b> /+0.63
Mg(001)	- <b>6.22</b> /-5.81	- <b>6.74</b> /-5.60	-6.98/- <b>7.42</b>	-7.48/- <b>7.60</b>	-5.84/-5.84	- <b>6.08</b> /-6.04	- <b>4.12</b> /-4.12	- <b>3.89</b> /-3.85
Sc(001)	-7.93/- <b>8.37</b>	-7.28/- <b>8.37</b>	-9.16/- <b>9.30</b>	-9.07/- <b>9.29</b>	- <b>6.98</b> /-6.87	- <b>6.73</b> /-6.66	- <b>5.37</b> /-5.33	- <b>5.10</b> /-5.07
Ti(001)	- <b>8.07</b> /-8.01	-7.50/- <b>7.58</b>	- <b>8.90</b> /-8.62	- <b>8.31</b> /-8.19	- <b>6.54</b> /-6.33	- <b>6.46</b> /-6.28	- <b>5.10</b> /-5.02	- <b>4.44</b> /-4.35
Co(001)	-5.48/- <b>5.68</b>	-4.61/- <b>4.66</b>	-5.62/- <b>5.68</b>	-5.00/- <b>5.01</b>	-4.12/- <b>4.19</b>	-3.69/- <b>3.75</b>	- <b>3.71</b> /-3.71	- <b>0.96</b> /-0.96
Zn(001)	-3.46/- <b>3.53</b>	-1.73/- <b>1.76</b>	-4.61/- <b>4.73</b>	-3.19/- <b>3.19</b>	-3.82/- <b>3.85</b>	- <b>3.51</b> /-3.49	-2.86/- <b>2.89</b>	- <b>1.02</b> /-1.01
Y(001)	-7.69/- <b>8.12</b>	-7.06/- <b>8.25</b>	-9.03/- <b>9.10</b>	-8.99/- <b>9.17</b>	- <b>6.94</b> /-6.82	- <b>6.69</b> /-6.60	- <b>5.38</b> /-5.35	- <b>5.27</b> /-5.24
Zr(001)	- <b>8.05</b> /-7.95	-7.76/- <b>7.82</b>	- <b>8.84</b> /-8.53	- <b>8.41</b> /-8.21	- <b>6.46</b> /-6.32	- <b>6.41</b> /-6.25	-5.09/- <b>5.11</b>	- <b>4.90</b> /-4.84
Tc(001)	-6.05/- <b>6.46</b>	-5.19/- <b>5.40</b>	-6.02/- <b>6.56</b>	-5.76/- <b>6.09</b>	-4.27/- <b>4.49</b>	-3.94/- <b>4.08</b>	-4.02/- <b>4.03</b>	-2.16/- <b>2.26</b>
Ru(001)	-5.45/- <b>6.19</b>	-4.65/- <b>4.87</b>	-5.38/- <b>5.98</b>	-4.98/- <b>5.13</b>	- <b>4.14</b> <sup>b</sup> /-3.93	-3.54/- <b>3.59</b> <sup>b</sup>	- <b>3.85</b> /-3.80	- <b>1.81</b> /-1.72
Cd(001)	-2.69/- <b>2.75</b>	-1.18/- <b>1.19</b>	-4.05/- <b>4.13</b>	- <b>2.94</b> /-2.93	-3.86/- <b>3.87</b>	- <b>3.63</b> /-3.62	-2.92/- <b>2.96</b>	- <b>1.80</b> /-1.78
Lu(001)	-8.03/- <b>8.52</b>	-7.32/- <b>8.59</b>	-9.44/- <b>9.58</b>	-9.35/- <b>9.55</b>	- <b>7.08</b> /-6.95	- <b>6.78</b> /-6.70	- <b>5.35</b> /-5.29	- <b>5.25</b> /-5.21
Hf(001)	- <b>8.43</b> /-8.34	-8.13/- <b>8.28</b>	- <b>9.22</b> /-8.77	- <b>8.77</b> /-8.49	- <b>6.54</b> /-6.20	- <b>6.49</b> /-6.21	- <b>5.08</b> /-4.93	- <b>4.90</b> /-4.78
Re(001)	-6.34/- <b>6.79</b>	-5.58/- <b>5.81</b>	-6.18/- <b>6.77</b>	-6.00/- <b>6.47</b>	-4.04/- <b>4.27</b>	-3.81/- <b>3.90</b>	-3.83/- <b>3.85</b>	-2.06/- <b>2.15</b>
Os(001)	-5.40/- <b>6.15</b>	-4.77/- <b>5.08</b>	-5.27/- <b>5.79</b>	-4.92/- <b>5.04</b>	- <b>3.66</b> /-3.50	-3.98 <sup>b</sup> /-3.98 <sup>a</sup>	- <b>3.52</b> /-3.42	- <b>1.70</b> /-1.60
Hg(001)	-1.29/- <b>1.98</b>	-1.75/- <b>1.87</b>	-3.03/- <b>3.03</b>	-3.06/- <b>3.10</b>	- <b>3.18</b> /-2.46	- <b>2.93</b> /-2.78	- <b>2.24</b> /-1.75	- <b>2.05</b> /-2.01
Tl(001)	- <b>3.44</b> /-3.29	-2.66/- <b>2.70</b>	-4.14/- <b>4.24</b>	- <b>3.87</b> /-3.87	- <b>4.14</b> /-4.10	-4.13/- <b>4.14</b>	- <b>3.19</b> /-3.15	- <b>2.94</b> /-2.93

<sup>a</sup> The reported value is for the more stable top site.

<sup>b</sup> The reported value is for the more stable bridge site.

**TABLE S6:** As in Table S1, but for the hollow sites on sc(100) surfaces. Note that only Bi is considered as a simple-cubic metal for the reasons explained in the main text. All values are in eV/adatom.

Surface	N <sub>ads</sub>		O <sub>ads</sub>		F <sub>ads</sub>		Cl <sub>ads</sub>	
	(2 × 2)	(1 × 1)	(2 × 2)	(1 × 1)	(2 × 2)	(1 × 1)	(2 × 2)	(1 × 1)
Bi(100)	-2.29	-3.13	-3.14	-4.21	-4.16 <sup>a</sup>	-3.20	-2.42	-2.07

<sup>a</sup> Adatom relaxed to top site (hollow site is unstable)

**TABLE S7:** List of exceptions, where the adatoms do not preferentially adsorb into “default” hollow sites; for fcc(111) the fcc site is considered as the default hollow site.  $E_b$  values of  $(1 \times 1)$  and  $(2 \times 2)$  overlayers of adatoms adsorbed on the default hollow site are compared to those on the alternative site, which is the most stable for at least one considered overlayer. All values are in eV/adatom.

adsorbate/surface system	default hollow site	$E_b$		alternative site	$E_b$	
		$(2 \times 2)$	$(1 \times 1)$		$(2 \times 2)$	$(1 \times 1)$
F/Al(111)	fcc	-4.78	-4.95	top	-5.05	-4.59
Cl/Al(111)	fcc	-3.33	-2.40	top	-3.52	-2.20
O/Al(100)	hollow	-5.96	-6.65	bridge	-6.60	-6.53
F/Al(100)	hollow	-4.22	-5.29	bridge	-5.23	-5.29
Cl/Al(100)	hollow	-3.10	-2.53	bridge	-3.55	-2.86
O/Ca(111)	fcc	-8.36	-7.93	hcp	-8.57	-8.48
F/Ca(111)	fcc	-6.86	-6.80	hcp	-7.00	-6.87
Cl/Ca(111)	fcc	-5.29	-5.27	hcp	-5.37	-5.31
Cl/Mn(110)	hollow	-5.80	/	top	/	-1.43
Cl/Fe(110)	hollow	-3.33	/	top	-3.76	-1.57
O/Fe(100)	hollow	-5.08	-5.64	bridge	-5.25	-5.64
F/Fe(100)	hollow	-2.51	-4.05	bridge	-5.31	-4.46
Cl/Fe(100)	hollow	-2.74	-3.07	bridge	-3.42	-3.20
N/Sr(111)	fcc	-6.65	-6.48	hcp	-6.77	-6.29
O/Sr(111)	fcc	-8.06	-7.64	hcp	-8.45	-8.36
F/Sr(111)	fcc	-6.82	-6.71	hcp	-7.01	-6.78
Cl/Sr(111)	fcc	-5.34	-5.31	hcp	-5.47	-5.35
F/Ru(001)	fcc	-4.03	-3.54	bridge	-4.14	-3.59
F/W(110)	hollow	-4.77	-4.60	top	-5.15	-4.87
F/Os(001)	fcc	-3.66	/	top	-4.10	-3.98
F/Ir(111)	fcc	-3.12	/	top	-3.64	-3.42
Cl/Ir(111)	fcc	-3.04	/	top	-3.05	-2.07
F/Pt(111)	fcc	-2.62	/	top	-3.13	-2.74
F/Bi(100)	hollow	/	-3.20	top	-4.16	-3.36

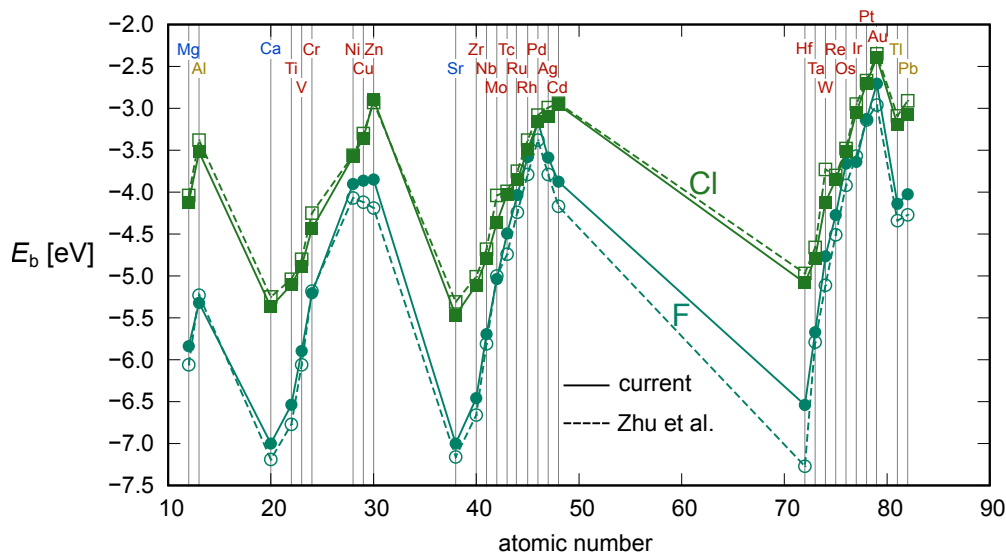


**Figure S11.**  $E_b$  values for  $(2 \times 2)$  overlayers of F and Cl adatoms on close-packed metal surfaces obtained in the present study (solid lines and filled symbols) as compared to  $E_b$  values for F and Cl reported by Zhu et al.<sup>2</sup> (dashed lines and open symbols). Lines are drawn to guide the eye.

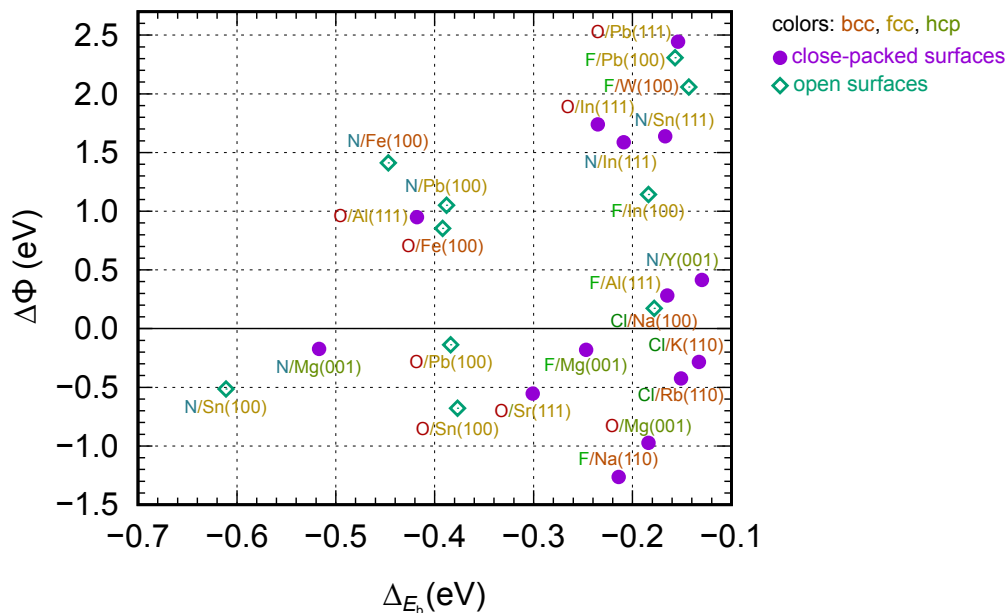
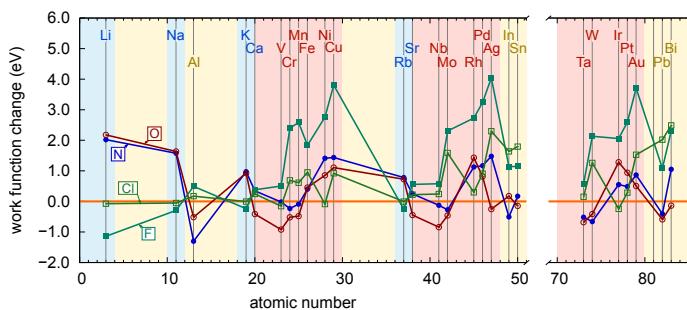


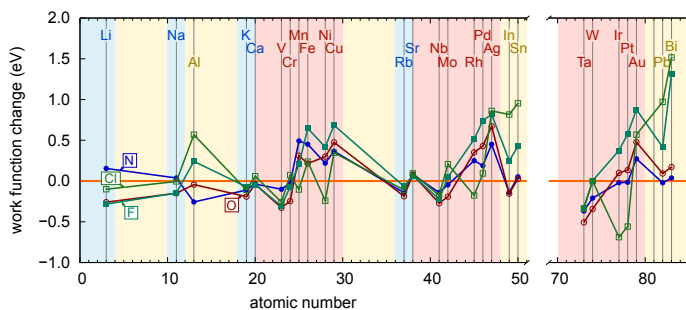
**Figure S12.** Adsorption induced work function change ( $\Delta\Phi$ ) of  $(1 \times 1)$  adatom overlayers for all identified cases of attractive lateral interactions ( $\Delta E_b < -0.1$  eV), whereas adsorption induced work function changes of all considered adatom overlayers are shown in Figure S13.



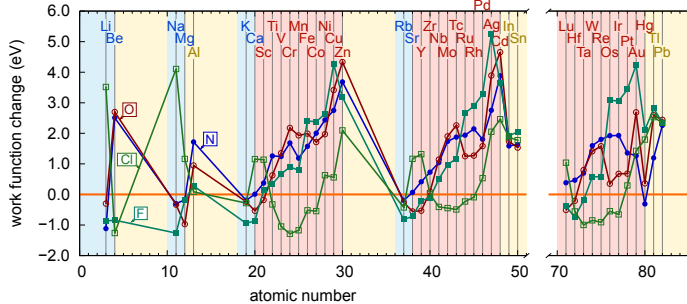
(a) (1×1) overlayers, open surfaces



(b) (2×2) overlayers, open surfaces



(c) (1×1) overlayers, close-packed surfaces



(d) (2×2) overlayers, close-packed surfaces

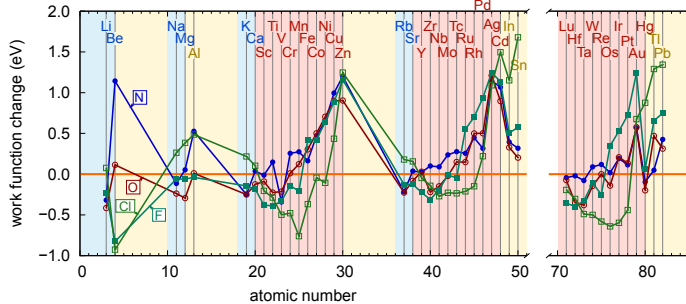


**Figure S13.** Adsorption induced work function change for all considered (1 × 1) and (2 × 2) adatom overlayers. The lines are drawn to guide the eye.

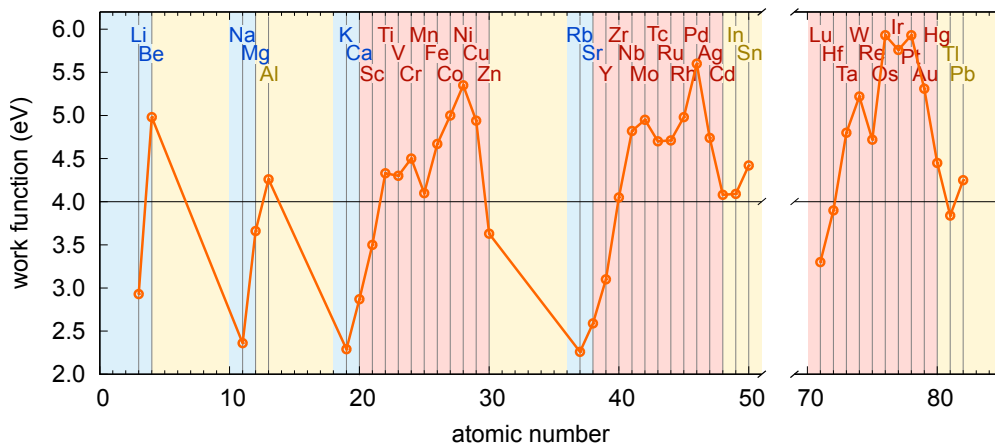


**Figure S14.** Experimental work functions of metals considered in this study; data are taken from Ref. 6. Where available the work function for the close-packed surface is plotted, otherwise the polycrystalline value is used. The lines are drawn to guide the eye.